Since January 2020 Elsevier has created a COVID-19 resource centre with free information in English and Mandarin on the novel coronavirus COVID-19. The COVID-19 resource centre is hosted on Elsevier Connect, the company's public news and information website.

Biophysical and structural characterizations of the effects of mutations on the structure–activity relationships of SARS-CoV-2 spike protein

Pei-Yu Yu[a], Tzu-Jing Yang[a], and Shang-Te Danny Hsu[a,b,*]
[a]Institute of Biological Chemistry, Academia Sinica, Taipei, Taiwan
[b]Institute of Biochemical Sciences, National Taiwan University, Taipei, Taiwan
*Corresponding author: e-mail address: sthsu@gate.sinica.edu.tw

Contents

Methods in Enzymology
ISSN 0076-6879
https://doi.org/10.1016/bs.mie.2022.07.013

Abstract

Mutations on the spike (S) protein of SARS-CoV-2 could induce structural changes that help increase viral transmissibility and enhance resistance to antibody neutralization. Here, we report a robust workflow to prepare recombinant S protein variants and its host receptor angiotensin-convert enzyme 2 (ACE2) by using a mammalian cell expression system. The functional states of the S protein variants are investigated by cryo-electron microscopy (cryo-EM) and negative staining electron microscopy (NSEM) to visualize their molecular structures in response to mutations, receptor binding, antibody binding, and environmental changes. The folding stabilities of the S protein variants can be deduced from morphological changes based on NSEM imaging analysis. Differential scanning calorimetry provides thermodynamic information to complement NSEM. Impacts of the mutations on host receptor binding and antibody neutralization are *in vitro* by kinetic binding analyses in addition to atomic insights gleaned from cryo-electron microscopy (cryo-EM). This experimental strategy is generally applicable to studying the molecular basis of host-pathogen interactions.

Abbreviations

3DVA	three-dimensional variability analysis
ACE2	angiotensin-convert enzyme 2
BLI	biolayer interferometry
Cryo-EM	cryo-electron microscopy
CTF	contrast transfer function
CV	column volume
DMSO	dimethyl sulfoxide
DSC	differential scanning calorimetry
FP	fusion peptide
FPLC	fast protein liquid chromatography
HR	heptad repeat
NSEM	negative staining electron microscopy
NTD	N-terminal domain
PCR	polymerase chain reaction
PEI	polyethyleneimine
RBD	receptor-binding domain
RBM	receptor-binding motif
S	spike
SARS-CoV-2	severe acute respiratory syndrome coronavirus 2
SEC	size-exclusion chromatography
TM	transmembrane
UF	uranyl formate
VOC	variant of concern
VOI	variant of interest

1. Introduction

The emergence of severe acute respiratory syndrome coronavirus 2 (SARS-CoV-2) is responsible for the COVID-19 pandemic that has, as of April 2022, led to more than 500 million confirmed cases and claimed more than six million lives. Since the first identification of the original SARS-CoV-2 strain in China at the end of 2019, several variants of concern (VOCs), namely the Alpha, Beta, Gamma, Delta, and, more recently, the Omicron variant, have been identified in different parts of the world. These VOCs exhibit increased viral transmissibility (Lyngse et al., 2021; Mlcochova et al., 2021; Ozono et al., 2021; Plante et al., 2021) and enhanced resistance to antibody neutralization (Corti, Purcell, Snell, & Veesler, 2021; Liu et al., 2022; Planas et al., 2021; Wang, Casner, et al., 2021; Wang, Nair, et al., 2021). Importantly, all VOCs harbor a D614G mutation in the spike (S) protein that was first identified in mid-April 2020. The Alpha variant was discovered in the United Kingdom in September 2020; the Beta and Gamma variants were identified in South Africa and Brazil in May 2020 and November 2020, respectively. In 2021, the Delta variant was reported in India together with the Kappa variant, which was designated as a variant of interest (VOI). The most recent and the most dominating VOC is the Omicron variant, which emerged in South Africa in November 2021. The Omicron variant has many mutations on the S protein, which are responsible for the surge in reinfections and breakthrough infection cases.

SARS-CoV-2 is an enveloped virus whose surface is decorated with highly glycosylated S proteins anchored onto the membrane through a single transmembrane helix. S protein consists of two subunits, namely the S1 and S2 subunits (Walls et al., 2020; Wrapp et al., 2020). The S1 subunit binds to the host receptor angiotensin-convert enzyme 2 (ACE2) *via* the receptor-binding domain (RBD), thereby triggering a series of conformational changes to the mediate membrane fusion with the host achieving viral entry to achieve viral entry (Fan, Cao, Kong, & Zhang, 2020; Ke et al., 2020; Shang et al., 2020). Effective ACE2 binding requires the opening of the RBD in an upward conformation to make the receptor-binding motif (RBM) accessible. As such, the RBD is also targeted by antibodies that sterically prevent ACE2 binding from achieving potent neutralization (Barnes, West, et al., 2020; Cao et al., 2020; Liu et al., 2020; Piccoli et al., 2020; Su et al., 2021; Yang et al., 2020). Another highly immunogenic region within the S protein is the N-terminal domain (NTD) that harbors a supersite

(Cerutti et al., 2021; Chi et al., 2020). Many mutations located in the RBD and NTD supersite can effectively render the VOCs and VOIs refractory to neutralizing monoclonal antibodies, thereby leading to immunity escape (Barnes, Jette, et al., 2020; Corti et al., 2021; Mannar et al., 2022; Wang, Casner, et al., 2021; Yang, Yu, Chang, Liang, et al., 2021). Understanding the molecular mechanism underlying the immunity escape of the individual VOCs and VOIs is therefore essential for the development of COVID-19 prevention and treatments and the fundamental understanding of viral infection and evolution.

In this chapter, we describe a robust experimental strategy to investigate the structure–function relationships of the S protein variants of SARS-CoV-2 by integrating cryo-electron microscopy (cryo-EM), negative staining electron microscopy (NSEM), differential scanning calorimetry (DSC), and biolayer interferometry (BLI) to obtain atomic insights into how mutations impact on the structures, stabilities, receptor binding and immunity escape. The integrated approach also helps reveal the unique cold denaturation propensity of the S protein variants that has direct implications on the development of S protein-based vaccines.

2. Key resources table

2.1 Molecular cloning

1. pcDNA™3.4 TOPO™ TA Cloning Kit (Invitrogen, Cat #14697)
2. Synthetic genes corresponding to the S protein variants are codon-optimized for HEK293 expression. The protein sequences of variants follow the definitions in PANGOLIN database (https://cov-lineages.org/resources/pangolin.html).
3. Polymerase chain reaction (PCR) thermocycler (Mastercycler EP Gradient S, Eppendorf)
4. PCR buffer and reagents: KOD Hot Start DNA polymerase Kit (Novagen), $MgSO_4$ (NEB), dNTPs (NEB), HindIII (NEB), EcoRI (NEB), DpnI (NEB), NEB3.1 (NEB), T4 ligase and T4 ligase buffer (NEB)
5. PCR clean-up kit (GenepHlow Gel/PCR kit, Cat #DFH100, Geneaid)
6. Eppendorf centrifuge (Thermo Fisher Scientific)
7. Sequence analysis software (SnapGene)
8. *E. coli* DH5α strain for plasmid amplication (ECOS™ 101, Yeastern Biotech)
9. Presto™ Mini plasmid extraction kit (Cat #PDH100, Geneaid)

10. EasyPrep EndoFree Maxi plasmid extraction kit (Cat #DPT-BA17, TOOLS)
11. UV–Vis spectrometer (Nano-photometer N60, IMPLEN)
12. Gel Loading Dye, Purple (6X) (Cat #B7024S, New England Biolabs)
13. SYBR safe DNA gel stain (Invitrogen)
14. GeneRuler 1 kb DNA ladder (Thermo Fisher Scientific)

2.2 Cell culture

1. Sterile laminar airflow cabinet (Thermo 1377, 1300 series A2)
2. Sterile water bath (TKS, IUB212-B2)
3. Freestyle™293 expression medium (Cat #12338026, Gibco)
4. Expi293™ expression medium (Cat #A1435102, Gibco)
5. Sterile 125 mL polycarbonate Erlenmeyer flask with a vented cap (Cat# 431143, Corning)
6. Sterile 1 L polycarbonate Erlenmeyer Flask with a vented cap (Cat #431147, Corning)
7. Sterile 2 L polycarbonate Erlenmeyer Flask with a vented cap (Cat #431255, Corning)
8. Pipette controller Midi Plus (Satorios)
9. Sterile serological pipet (Corning)
10. 1000, 10 μL pipettes and serological pipette (TPP)
11. 1.5 mL tube (Eppendorf)
12. Thermo Scientific large capacity CO_2 Incubator, Thermo 3950 (Thermo Fisher Scientific)
13. FreeStyle™ 293-F cells (Cat #R79007, Gibco)
14. Expi293F™ cells (Cat #A14527, Gibco)
15. Automated cell counter (TC20 Cat #1450102, Bio-Rad)
16. Cell counting slides (TC10™/TC20™ cell counter, dual-chamber, BIO-RAD)
17. Dimethyl sulfoxide (DMSO, Sigma, D2650–100 mL)
18. Cryovial (Corning)
19. Cryofreezing container (NALGENE)

2.3 Plasmid transfection

1. Purified plasmid DNA (in-house)
2. 50 mL centrifuge tube (Corning)
3. Phosphate buffered saline (PBS, gibco, 10,010–023)
4. Linear polyethyleneimine (PEI)

5. ExpiFectamine™293 transfection kit 1 L (Gibco)
6. Opti-MEM™ I reduced serum medium

2.4 Protein expression

1. 500 mL centrifuge tube (Corning)
2. Centrifuge (Beckman Coulter J6-MI, JS-4.2A)
3. Bottle top sterile filter (Thermo Fisher Scientific)

2.5 Protein purification

1. HisPur cobalt resin (Thermo Fisher Scientific)
2. Econo-Column chromatography columns, 2.5×20 cm (Cat #7372522, Bio-Rad)
3. Spike binding buffer containing 20 mM Tris, 150 mM NaCl, 10 mM imidazole, pH 8
4. Purification buffer containing 50 mM Tris, 150 mM NaCl, 0.02% NaN_3, pH 7.6
5. Spike wash buffer containing 20 mM Tris, 300 mM NaCl, 10 mM imidazole, pH 8
6. Spike elution buffer contained 20 mM Tris, 300 mM NaCl, 150 mM imidazole, pH 8
7. Size-exclusion chromatography column (Superose 6 Increase 10/300 GL or Superdex 200 16/60 pg, GE Healthcare)
8. Ion exchange column (HiPrep QFF, GE Healthcare)
9. Peristaltic pump P-1 (GE Healthcare)
10. Fast protein liquid chromatography (FPLC) system (ÄKTA Prime, UPC10 or PURE 25, GE Healthcare)
11. PageRuler™ Prestained Protein Ladder, 10–180 kDa (Cat #26616, Thermo Fisher Scientific)
12. 4–12% precast gel (SurePAGE, GeneScript)
13. Fluorescence imager (iBright, Thermo Fisher Scientific)

2.6 Biolayer interferometer (BLI)

1. Octet Red96 system (FORTÉBIO)
2. Octet® high precision streptavidin (SAX) biosensors (FORTÉBIO)
3. Zeba™ spin desalting columns, 7 K MWCO, 0.5 mL (Thermo Fisher Scientific)
4. 96-Well black microplate, polystyrene (Greiner Bio-One)

2.7 Negative stain electronic microscopy

1. Uranyl formate (UF, Polysciences)
2. EM grid (electron microscopy sciences, CARBON FILM 300 MESH, COPPER)
3. Tweezer (DUMONT)
4. Filter paper (ADVANTEC)
5. Glow discharge (PELCO easiGlow™)
6. cryoSPARC v2.14
7. 200 keV electron microscope (Tecnai G2-F20, FEI, the Netherlands)

2.8 Differential scanning calorimetry (DSC)

1. 50 mM Tris–HCl, 150 mM NaCl, and 0.02% NaN_3, pH 7.6.
2. Automatic MicroCal PEAQ-DSC (Malvern).

2.9 Cryo-electron microscopy

1. EM grid (300-mesh Quantifoil R1.2/1.3 holey carbon grids)
2. Filter paper (ADVANTEC)
3. Glow discharge (PELCO easiGlow™)
4. Vitrification system (Vitrobot Mark IV, Thermo Fisher Scientific)
5. Cryo-electron microscope (300 keV Titan Krios, Thermo Fisher Scientific)
6. Direct electron detector (Gatan Kr direct detector, Gatan)
7. cryoSPARC v2.14
8. RELION v.3.0
9. UCSF-Chimera v.1.14
10. UCSF-ChimeraX v.1.1.1
11. Coot v.0.93
12. Phenix v.1.18

3. Recombinant protein production

3.1 Molecular cloning

The ectodomain of the SARS-CoV-2 S protein (residues 1–1208; for simplicity, hereafter defined as S protein unless otherwise specified) is engineered to have a tandem proline replacement at residue positions 986–987, and furin cleavage site mutations at residue positions 682–685 (RRAR to GSAS) to stabilize the prefusion state as described previously (Pallesen et al., 2017).

1. Generate three PCR fragments from the original synthetic DNA template corresponding to the S protein using three specific primer pairs. Two stabilization mutations are intended to place into the part of primers, which create the overlapping regions (Fig. 1). The melting temperature of the overlapping region (or annealing region) is set to at least 60 °C

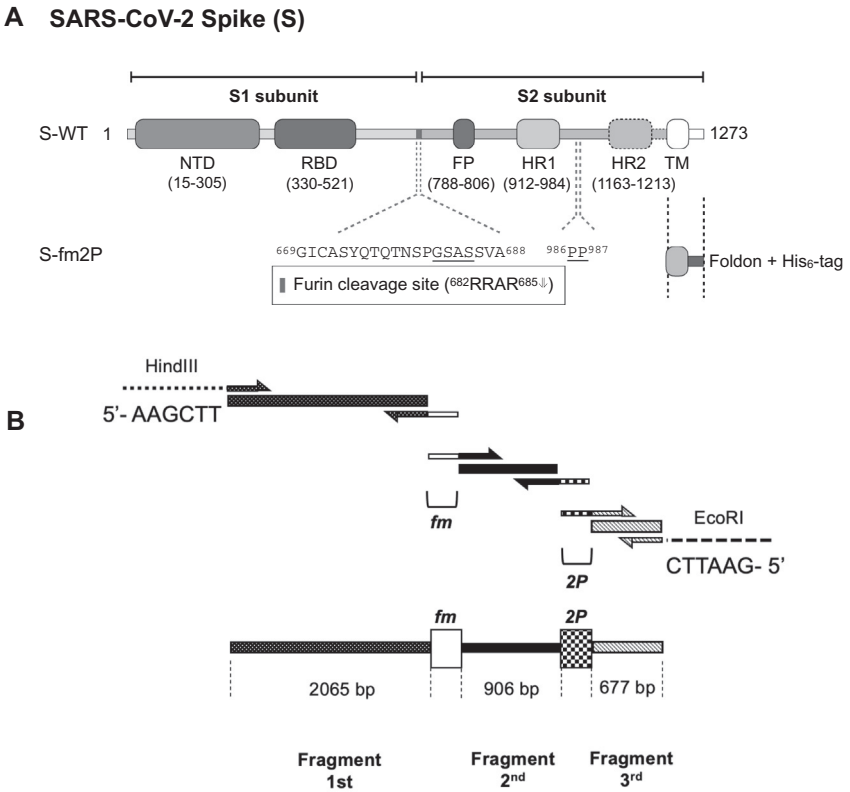

Fig. 1 Introduction of furin cleavage mutation and proline substitution on SARS-CoV-2 spike protein by overlapping PCR. (A) Domain architecture and stabilizing mutations of the S protein. Two sets of mutations were introduced to stabilize in the prefusion state, namely furin cleavage site mutation (fm) and tandem proline substitution (2P). The C-terminal domain of T4 fibritin (Foldon) was introduced to replace the transmembrane (TM) domain. NTD, N-terminal domain. RBD, receptor-binding domain. FP, fusion peptide. HR1 and HR2, heptad repeat 1 and 2. TM, transmembrane domain. (B) Three fragments generated by three individual runs of regular PCR with specific primers are shown in different coloring styles. By using the designed primers, mutations of the furin cleavage site (fm, residues 682–685) and proline substitution (2P, residues 986–987) were introduced into the two overlapping regions, respectively. The melting temperature of overlapping regions should be adjusted to match assembles (fragments). Three fragments were eventually fused by PCR using a forward primer used to generate the Fragment 1st and a reverse primer used to create the Fragment 3rd.

2. Extract the target PCR fragment cut from the DNA gel using the gel extraction kit

   (Removing the excessive primers from each end product is a critical step, which may create non-specific PCR products, reducing the successful rate of final fragment annealing.)
3. Fuse three PCR fragments by a final round of PCR with specific primers
4. Extract the PCR product from cutting the gel to purify the product
5. Create the sticky ends of the resulting PCR product (as the insert DNA) and mammalian expression vector pcDNA3.4 with two specific restriction enzymes, including HindIII and EcoRI, at 37 °C for 2.5 h (double digestion).
6. Examine the digestion product by 1% agarose gel electrophoresis
7. Cut and extract the specific bands corresponding to the insert DNA and vector from the gel
8. Ligate the insert DNA and vector with T4 ligase at 16 °C overnight
9. Perform the transformation by adding 10 μL ligation product into 50 μL *E. coli* DH5α competent cells in a 1.5-mL tube
10. Incubate the mixture on ice for 30 min
11. Heat shock the mixture at 42 °C for 45 s to increase the permeability of cell membrane, leading to the entry of the DNA (ligation product) to competent cells
12. Put the tube back on ice for 5 min
13. Add 500 μL fresh LB medium (without antibiotics) into the tube and incubate at 37 °C for 1 h
14. Streak 100 μL transformed cells on the LB agar plate with appropriate antibiotics
15. Incubate the plate at 37 °C overnight for growing the transformants
16. Inoculate multiple single colonies in 5 mL fresh LB medium and incubate at 37 °C with 180 rpm shake speed overnight
17. Sequence the selected individual colonies with appropriate primer pairs to ensure the successful insertion of the target genes into the expression vector

3.2 Expression of S protein variants in HEK293 freestyle cells

1. Pre-warm Freestyle™293 expression medium at 37 °C in a water bath
2. Take a vial of frozen HEK293 cells (cell stock: 2×10^7 cells/mL, 1 mL) from liquid nitrogen and thaw them at 37 °C by a water bath

3. Inoculate the cells in 30 mL pre-warned medium, and allow them to recover at 37 °C and 125 rpm, with 8% CO_2 for 24 h
4. Inoculate the cell culture to the target culture volumes (0.3, 0.6 or 1.2 L) with a cell density of 0.3–1.5 × 10^6 cells/mL. The cell density doubling time is about 24 h
5. Dilute the cell culture to a target density of 0.7 × 10^6 cells/mL 24 h before transfection
6. On the day of transfection, the cell density is expected to be 1–1.5 × 10^6 cells/mL with over 95% cell viability
7. Add 300 μg plasmid DNA into 15 mL PBS buffer and incubate at room temperature for 5 min
8. Add 600 μg polyethyleneimine (PEI) into 15 mL PBS buffer and incubate at room temperature for 5 min
9. Mix the plasmid DNA and PEI/PBS solutions and incubate at room temperature for 20 min
10. Add the DNA/PEI mixture to the cell culture and incubate at 37 °C, 125 rpm with 8% CO_2 for 3 days
11. Add 50 mL pre-warmed fresh medium to the transfected cell culture 3 days post-transfection and continue for another 3 days under the same condition
12. Pellet the cells by centrifuge at 4000 rpm and 4 °C for 30 min. Harvest the medium by passing through the 0.22-μm filter cup

3.3 Purification of S protein variants

1. Add 10 × binding buffer (200 mM Tris–HCl, 1500 mM NaCl, 100 mM imidazole, pH 8.0) and 5 mL cobalt resins into the medium to initiate binding at 4 °C and 140 rpm overnight
2. Load the culture medium with cobalt resins into an Econo-Column Chromatography column and allow the resins to sediment by gravity
3. Carefully wash the resins with 10 column volumes (CVs) of wash buffer (20 mM Tris–HCl, 0.3 M NaCl, 10 mM Imidazole, pH 8.0).
4. Elute the target protein from the resins with 10 CVs of elution buffer (20 mM Tris–HCl, 0.3 M NaCl, 150 mM Imidazole, pH 8.0).
5. Concentrate the eluent by a 100-kDa cut-off concentrator (Amicon® Ultra-15 Centrifugal Filter Unit, 100 kDa) to a final volume of 500 μL. Filter the concentrate using 0.22-μm centrifugal filter (Nanosep® centrifugal filters, PALL).

6. Load the concentrate into a size-exclusion chromatography (SEC) column (Superose 6 increase 10/300 GL) for further purification

   Note: All the steps are performed at room temperature, except for the binding step at 4 °C overnight.
7. Collect the protein-containing fractions based on UV absorption profile of the SEC chromatogram, and confirm the identity and purity of individual fractions by SDS-PAGE (SurePAGE™, Bis-Tris, 10 × 8, 4–12%, 15 wells) stained by Coomassie blue (Fig. 2).
8. Concentrate the S protein-containing fractions, determine the corresponding protein concentration by using a UV–Vis spectrometer, and aliquot the concentrate to appropriate volumes for storage

3.4 Expression of super-fold GFP-fused ACE2 ectodomain (sfGFP-ACE2) in Expi293 cells

1. Pre-warm Expi™293 expression medium at 37 °C in a water bath
2. Take a vial of Expi293 cells (cell stock: 2×10^7 cells/mL, 1 mL) from liquid nitrogen, and thaw it at 37 °C in a water bath
3. Transfer the cells to 30 mL of pre-warmed medium, and allow them to recover at 37 °C and 125 rpm, with 8% CO_2 for 24 h.
4. Gently pellet the cells by centrifuge at 700 rpm and 4 °C for 5 min. Decant the supernatant and resuspend the cell pellet with fresh medium to a culture volume with a typical cell density of 0.5×10^6 cells/mL
5. Inoculate the cell culture to the target culture volumes with a cell density of 2×10^6 cells/mL on the day before transfection
6. Verify the cell density to be 3–3.5 × 10^6 cells/mL with a cell viability over 95% before transfection
7. Add 30 μg plasmid DNA Prepare into 1.5 mL Opti-MEM medium and incubate at room temperature for 5 min
8. Add 81 μL ExpiFectamine into 1.5 mL Opti-MEM medium and incubate at room temperature for 5 min
9. Mix the DNA and ExpiFectamine solutions and incubate at room temperature for 20 min
10. Add the DNA/ExpiFectamine mixture to the cell culture (typically 30 mL in volume), and incubate at 37 °C, 125 rpm with 8% CO_2 for 20 h
11. Add 150 μL enhancer I and 1.5 mL enhancer II to the cell culture 20 h post-transfection and continue cell culture at 37 °C, 125 rpm with 8% CO_2 for another 4 days

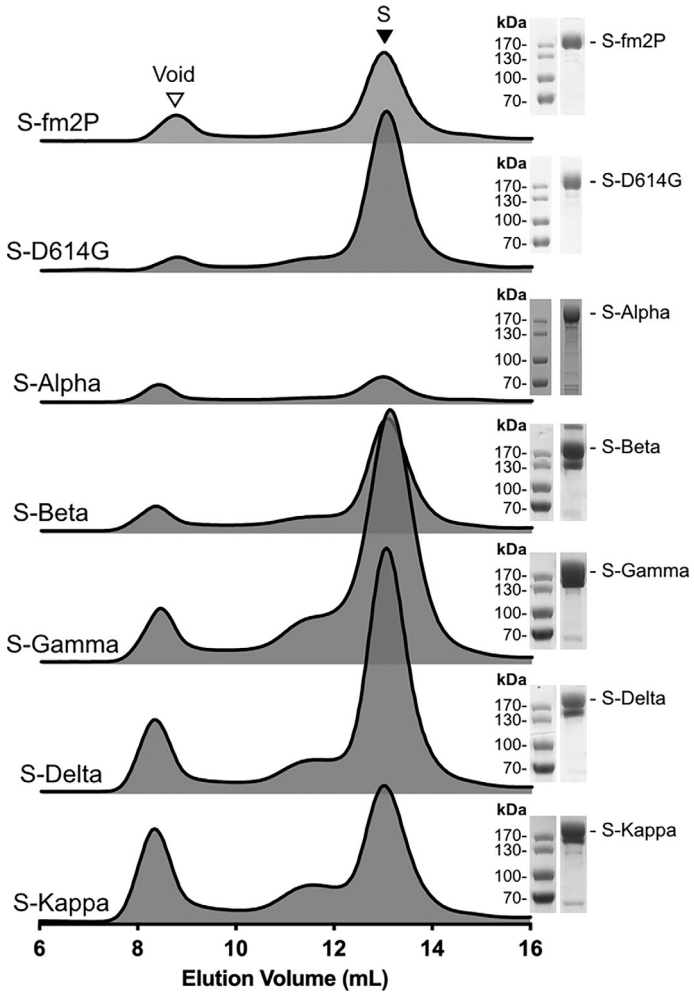

Fig. 2 Purification of S protein variants. SEC profiles of different S protein variants, namely S-fm2P, S-D614G, S-Alpha, S-Beta, S-Gamma, S-Delta and S-Kappa in descending order. The position of the main elution peaks that correspond to the S protein variants in their trimeric states is indicated by an arrow. The resulting protein samples were analyzed by a 4–12% gradient SDS-PAGE, stained by Coomassie blue (right panel). The positions of the individual S protein variants are indicated.

12. Transfer the cell culture to a 50 mL centrifuge tube for harvesting
13. Pellet the cells by centrifuge at 2000 rpm and 4 °C for 20 min. Collect the cell culture medium by filtering through a 0.22-μm membrane to a sterile 100 mL serum bottle

Note: The samples are kept in the dark at all times to prevent GFP fluorescence quenching.

3.5 Purification of sfGFP-ACE2

1. Add 10 × binding buffer (500 mM Tris–HCl, pH 7.4, 250 mM NaCl) to the cell medium before loading to an anion exchange column (HiTrap Q FF) by using the Peristaltic Pump P-1 at a flow rate of 2 mL/min
2. Elute the target protein by a linear gradient of sodium chloride (0–1 M) in the presence of 50 mM Tris–HCl, pH 7.4
3. Collect the protein-containing fractions and confirm their identities and purities by running a precast 4–12% linear gradient SDS-PAGE, followed by taking a fluorescence image of the gel (iBright Imaging System, Thermo Fisher Scientific) based on the GFP signal
4. Pool the sfGFP-ACE2 containing fractions and concentrate to a final volume of 2 mL for SEC purification using a prep grad SEC column (Superdex 200 16/60, GE Healthcare).
5. Collect the sfGFP-ACE2 containing fractions (they are visibly green) and run a 4–12% SDS PAGE to confirm their identities and purities by GFP fluorescence imaging, followed by Coomassie blue staining (Fig. 3).

4. Thermal stability analyses of S protein variants

S protein variants are marginally thermostable, and they are sensitive to storage conditions. To evaluate the impacts of mutations on the folding stabilities of S protein variants, we use differential scanning calorimetry (DSC; MicroCal PEAQ-DSC Automatic system, Malvern) to quantify their melting temperatures and enthalpy of unfolding under different experimental conditions.

1. The concentrations of individual S protein variants are set to 0.2 mg/mL in 50 mM Tris–HCl (pH 7.6), 150 mM NaCl, and 0.02% NaN_3
2. The sample temperature is ramped up from 10 to 90 °C at a rate of 200 °C/h
3. The resulting data were baseline-corrected by the built-in software of MicroCal PEAQ-DSC, and exported to GraphPad Prism 9 to replot the graphs
4. The melting temperatures (T_m) and enthalpy of unfolding (ΔH) are deduced by the built-in software

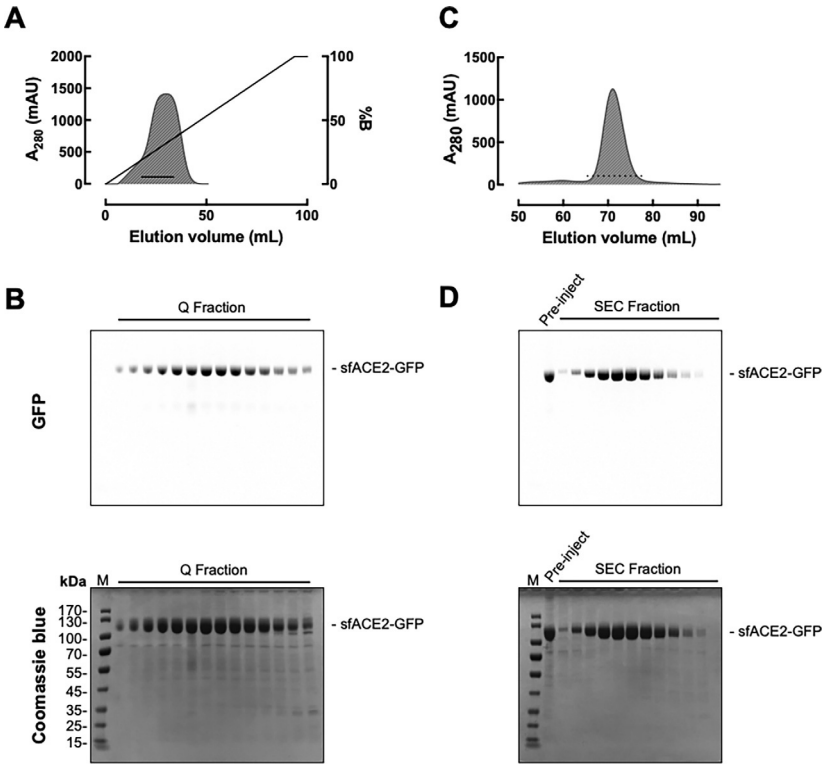

Fig. 3 Purification of sfACE2-GFP. (A) Anion exchange chromatogram of sfACE2-GFP. The linear NaCl gradient from 0 to 1 M is indicated by a straight line with the corresponding concentration in the percentage of buffer B (1 M NaCl) indicated on the right Y-axis. (B) Fluorescence image and Coomassie blue staining of the SDS-PAGE of the individual elution fractions derived from (A). (C) Size-exclusion chromatogram of sfACE2-GFP separated by a Superdex 200 16/60 SEC column. The dotted lines indicate the positions of the individual fractions collected and analyzed by SDS-PAGE. (D) Fluorescence image and Coomassie blue staining of the SDS-PAGE of the individual elution fractions derived from (C).

5. Folding stability analyses of S protein variants by NSEM

In addition to the global thermodynamics analysis by DSC, which reports on the global thermal unfolding events, we use NSEM to monitor morphological changes of S protein variants under different experimental

conditions to provide additional structural information with regard to the folding stabilities and local unfolding events that is otherwise inaccessible to DSC and other biophysical analyses.

1. Clamp the edge of the grids using a negative tweezer, then put it on the glass slide and place it into the glow discharger. Hydrophilize and clean the surface of the carbon-coated EM grid with glow discharge treatment at 25 mA for 30 s
2. Apply four microliters of S protein solution at a concentration of 50 μg/mL onto the EM grid. Wait for 1 min to allow the sample to spread evenly on the grid surface
3. Blot away the protein solution from the grid with a filter paper against the edge of the grid
4. Stain the grid with four microliters of 2% uranyl formate (UF) and incubate for 1 min
5. Blot away excess UF with a filter paper against the edge of the grid, and dry the grid in the air for a few minutes. Store the grid in the grid box for further usage

   Note: Typically, the grid left in the air overnight to complete dryness before data collection.
10. Collect NSEM data using a 200 keV FEI Tecnai G2-F20 electron microscope with the magnification of 50,000×, corresponding to a pixel size of 1.732 Å. A typical NSEM dataset of apo S protein variants consists of 60 micrographs, and that of antibody-bound S protein variants consists of 240 micrographs
11. Load the NSEM dataset into cryoSPARC for contrast transfer function (CTF) correction, followed by particle picking using the "Blob Picker" function with a box size of 224 pixels on each side
12. Use two-dimensional (2D) class averaging to iteratively select native-like particle images
13. Reconstruct *ab-initio* three-dimensional (3D) models (class = 3) without imposing symmetry (C1) constrains using the 2D classification selected particle images
14. Perform heterogeneous refinement with the resulting *ab-initio* 3D models to generate three EM maps
15. Visualize the resulting EM maps using UCSF-Chimera (Pettersen et al., 2004) or UCSF-Chimera X (Pettersen et al., 2021)

    Note: 3D classification can help filter poor particle images that cannot be easily identified by the 2D classification step (see Fig. 4).

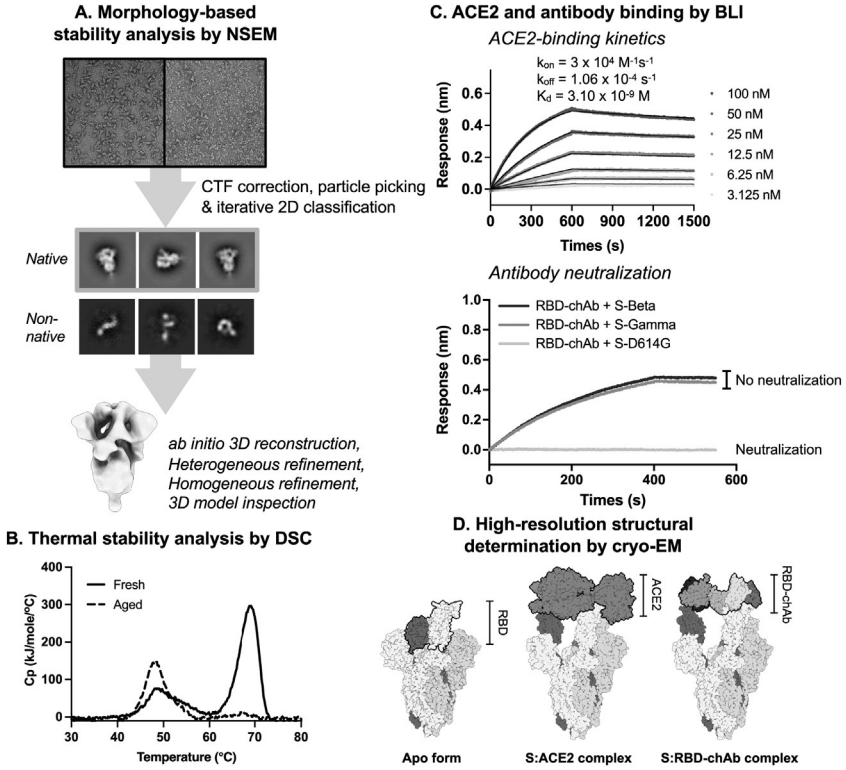

Fig. 4 Characterizations of the structures, stabilities, and functions of S protein variants. (A) The top panel shows two representative NSEM micrographs of S protein variants. The middle panel shows two sets of 2D class-averaged images of S protein variants. The upper one corresponds to the native-like particles with well-defined secondary structural elements and a compact trimeric structure. The lower one corresponds to non-native particle images with ill-defined particle morphologies. The native-like particle images are further processed to generate 3D EM maps, as shown in the bottom panel. The numbers of native-like particle images after the 2D/3D image analyses quantify the number of native spike particles retained after different experimental treatments. (B) Representative DSC profiles of fresh (solid line) and aged (dashed line) samples. The loss of the high-temperature transition peak in the aged sample (cold storage at 4 °C for 6 days) underscores the loss of stability due to cold denaturation. (C) Representative BLI results of direct ACE2 binding (upper panel) and antibody neutralization assay (lower panel). A neutralizing antibody (RBD-chAb) can effectively block ACE2 binding to the D614G variant (S-D614G) but fails to neutralize ACE2 binding by the Beta and Gamma variants (S-Beta and S-Gamma), evidenced by the signal build-up for the two variants. (D) Representative cryo-EM maps of S proteins in their apo, ACE2-bound, and antibody-bound forms. The RBD, ACE2, and neutralizing antibodies (RBD-chAb) structures are outlined by thick black lines.

6. Kinetic analysis of receptor and antibody binding to S protein variants

We use BLI to evaluate how the mutations in the S protein variants affect ACE2 binding and antibody neutralizing of ACE2 binding. BLI analyses report on the kinetic rate constants of the association (k_{on}) and dissociation (k_{off}) of binding partners, and the ratio of which is the dissociation constant ($K_d = k_{off}/k_{on}$) that describes the binding affinity. Typically, sfGFP-ACE2 is immobilized onto the BLI sensor to probe its binding to S protein variants of a range of concentrations. To assess the neutralizing capacity of monoclonal antibodies against ACE2 binding to the S protein variants, the antibodies are preincubated with the S protein variants before carrying out the competitive ACE2 binding assays. Effective neutralizing antibodies are expected to prevent ACE2 binding to the S protein variants manifested in the lack of signal build-up in the BLI experiments (Fig. 4).

In the following protocol, steps 1–4 are required to biotinylate the sfGFP-ACE2. Steps 5–6 are performed to immobilize biotinylated sfGFP-ACE2 onto the BLI SAX biosensor for the direct binding experiments (step 7), and antibody competition (neutralization) experiments (step 8).

1. Incubate sfACE2-GFP with NHS-LC–LC-biotin at a molar coupling ratio (MCR) of 3:1 (3 biotin for every sfACE2-GFP molecule) for 30 min on ice
2. Equilibrate a Zeba™ Spin Desalting Column with 50 mM Tris–HCl (pH 7.6), 150 mM NaCl, 0.02% NaN_3
3. Load the biotinylated product into the desalting column to remove the excessive labeling agent in the appropriate reaction buffer
4. Determine the molar concentration of the biotinylated sfACE2-GFP by using a UV–Vis spectrometer and store it at 4 °C until further use
5. Before the BLI experiment, transfer the Octet® High Precision Streptavidin (SAX) biosensors to a flat-bottom and 96-well black microplate filled with assay buffer (50 mM Tris–HCl,150 mM NaCl, 0.02% NaN_3, 0.01% BSA, pH 7.6) to hydrate the biosensors for 30 min
6. Immobilize the biotinylated sfGFP-ACE2 onto the SAX biosensors and quench the immobilization with biocytin (biotinyl-lysine, 50 μg/mL).
7. For direct ACE2 binding analyses, serially diluted S protein solutions (100, 50, 25, 12.5, 6.25, 3.125 nM in assay buffer 50 mM Tris–HCl, 150 mM NaCl, 0.02% NaN_3, 0.01% BSA, pH 7.6) are used to carry

independent BLI experiments with fresh and independent BLI biosensors. The BLI experiments are carried out at 25 °C with the association and dissociation periods set to 600 and 900 s, respectively

8. For antibody neutralization assays, 50 nM of S protein variants are incubated with monoclonal antibodies at a 1:1 M ratio at room temperature for 1 h. The BLI experiments are carried out at 25 °C with the association and dissociation periods set to 400 and 150 s, respectively
9. Analyze the data using the built-in software Data Analysis v10 (ForteBio) and replot them by using Prism 9 (GraphPad).

7. Structure–activity relationship analysis of s protein variants by cryo-EM

To examine how the mutations of VOCs and VOIs impact the structures of S protein variants and their functionalities, we use cryo-EM to determine the atomic structures of the S protein variants in three different functional states, namely their apo forms, receptor ACE2-bound forms, and neutralizing antibody-bound forms. These functional states are highly dynamic and generally exhibit abundant conformational heterogeneity. First, the RBD of the S proteins can interconvert between the open (up) and closed (down) conformations, and their relative populations can be modulated by the mutations within the S proteins. Second, the RBD and RBM mutations can alter the molecular interactions with receptor ACE2, thereby modulating the host binding affinity and, therefore, transmissibility. Third, the mutations in the RBD and RBM and those in the NTD can disrupt the structural epitopes used by different neutralizing antibodies against SARS-CoV-2, thereby leading to immunity escape. In many cases, a single cryo-EM sample can exhibit multiple conformations with different numbers of RBD in the up/down conformations and different numbers of RBD in the ACE2/antibody-bound state. To address the issue of conformational heterogeneity, advanced cryo-EM imaging processing tools are used. We use a combination of RELION and cryoSPARC to maximize the information content of the resulting EM maps. For cryoSPARC, we extensively use the 3D variability analysis (3DVA) module to extract structural information of the heterogeneous systems. For detailed descriptions of the cryo-EM data processing procedures of RELION and cryoSPARC, the readers are referred to the authors' original publications (Punjani & Fleet, 2021; Punjani, Rubinstein, Fleet, & Brubaker, 2017; Scheres, 2012, 2016). We shall briefly describe below the procedures for cryo-EM sample preparation and data processing specific to the studies on S protein variants.

1. Equilibrate the chamber of Vitrobot Mark IV to 100% humidity at 4 °C
2. Glow discharge a 300-mesh Quantifoil R1.2/1.3 holey carbon grids at 20 mA for 30 s to make the grid hydrophilic and clean
3. Load the EM grid with the aid of the Vitrobot tweezer into the Vitrobot Mark IV
4. Apply three microliters of protein solution to the grid and incubate for 30 s
5. Blot the grid for 2.5 s (Bolt force: 0).
6. Plunge-freeze the EM grid into liquid ethane cooled by liquid nitrogen
7. Clip grids and store them in liquid nitrogen until data collection
8. Collect the images using a 300 keV Titan Krios microscope (ThermoFisher Scientific) equipped with a Gatan K3 direct detector (Gatan) in a super-resolution mode using the EPU software (ThermoFisher Scientific).
9. Analyze the dataset by using a combination of RELION (Scheres, 2012, 2016) and cryoSPARC (Punjani et al., 2017; Punjani & Fleet, 2021) with a special focus on the conformational heterogeneity of the RBD by using the 3DVA module of cryoSPARC.
10. Visualize the resulting EM maps using UCSF-Chimera (Pettersen et al., 2004) or UCSF-Chimera X (Pettersen et al., 2021).
11. Generate an initial model by Swiss-Model using a S protein PDB structure as a template. The atomic coordinates are divided into individual domains and manually fit into the cryoEM maps by using UCSF-Chimera and UCSF-ChimeraX, and Coot (Emsley, Lohkamp, Scott, & Cowtan, 2010).
12. After iterative refinements, the structural models are refined by the real-space refinement module within Phenix (Adams et al., 2010).
13. The resulting structural models are used manually inspected and compared with other S protein structures to evaluate the structure–activity relationships of the individual S protein variants

8. Concluding remarks

The methods described herein outline the essential steps for *in vitro* biophysical characterizations of the S protein variants in terms of their thermostabilities, molecular structures, and impacts of clinically observed mutations in the VOCs and VOIs on the structure–activity relationships of the S protein variants. During our endeavor to investigate the effects of emerging VOC/VOI-associated mutations on the S protein, we discovered by serendipity the ability of the single D614G mutation to substantially reduce

sensitivity to cold storage-induced unfolding of the wild type S protein, making it not only less sensitive to cold denaturation but also more resistant to transient heat-induced unfolding (Yang, Yu, Chang, & Hsu, 2021). To this end, the integration of NSEM and DSC plays an essential role in providing quantitative descriptions with regard to the amount of native-like S protein variants retained after different stress/aging treatments. Such information would be key to vaccine developments based on recombinant S proteins. The integration of BLI and cryo-EM to investigate the structure–activity relationships of S protein variants is now widely used by the community, particularly in the context of the contributions of individual mutations to the host immunity escape of SARS-CoV-2 variants (Corti et al., 2021; Liu et al., 2022; Planas et al., 2021; Wang, Casner, et al., 2021; Wang, Nair, et al., 2021). Therefore, it is important to have a robust workflow to produce recombinant S protein variants using the mammalian cell expression system that ensures the post-translationally modified glycans on the recombinant S protein variants are as close to that of the authentic virus as possible (Amanat et al., 2020). Since the VOC/VOI-associated mutations can significantly modulate the intrinsic propensity of the RBD to populate the open conformation accessible to the ACE2 binding (Yang, Yu, Chang, & Hsu, 2021; Yang, Yu, Chang, Liang, et al., 2021), one should carefully assess the conformational heterogeneity of the S protein variants. Detailed accounts of the effects of the VOC-associated mutations on the structure–activity relationships of the S protein variants are beyond the scope of this chapter. Nevertheless, this chapter provides a general protocol that is adaptable to investigations of the molecular basis of other host-pathogen interaction systems to help provide structural and thermodynamic insights pertinent to antiviral developments for therapeutics and preventions.

Acknowledgments

This work is supported by an Academia Sinica Career Development Award (AS-CDA-109-L08), the Infectious Disease Research Supporting Grants (AS-IDR-110-08 and AS-IDR-111-03), and the Ministry of Science and Technology (MOST), Taiwan (MOST 110-2113-M-001-050-MY3 and MOST 110-2311-B-001-013-MY3) to S.-T.D.H..

References

Adams, P. D., Afonine, P. V., Bunkoczi, G., Chen, V. B., Davis, I. W., Echols, N., et al. (2010). PHENIX: a comprehensive Python-based system for macromolecular structure solution. *Acta Crystallographica. Section D, Biological Crystallography*, *66*, 213–221. https://doi.org/10.1107/S0907444909052925.

Amanat, F., Stadlbauer, F., Strohmeier, S., Nguyen, T. H. O., Chromikova, V., McMahon, M., et al. (2020). A serological assay to detect SARS-CoV-2 seroconversion in humans. *Nature Medicine*, *26*, 1033–1036. https://doi.org/10.1038/s41591-020-0913-5.

Barnes, C. O., Jette, C. A., Abernathy, M. E., Dam, K. A., Esswein, S. R., Gristick, H. B., et al. (2020). SARS-CoV-2 neutralizing antibody structures inform therapeutic strategies. *Nature*, *588*, 682–687. https://doi.org/10.1038/s41586-020-2852-1.

Barnes, C. O., West, A. P., Jr., Huey-Tubman, K. E., Hoffmann, M. A. G., Sharaf, N. G., Hoffman, P. R., et al. (2020). Structures of human antibodies bound to SARS-CoV-2 spike reveal common epitopes and recurrent features of antibodies. *Cell*, *182*, 828–842. https://doi.org/10.1016/j.cell.2020.06.025.

Cao, Y., Su, B., Guo, X., Sun, W., Deng, Y., Bao, L., et al. (2020). Potent neutralizing antibodies against SARS-CoV-2 identified by high-throughput single-cell sequencing of convalescent patients' B cells. *Cell*, *182*, 73–84. https://doi.org/10.1016/j.cell.2020.05.025.

Cerutti, G., Guo, Y., Zhou, T., Gorman, J., Lee, M., Rapp, M., et al. (2021). Potent SARS-CoV-2 neutralizing antibodies directed against spike N-terminal domain target a single supersite. *Cell Host & Microbe*, *29*, 819–833. https://doi.org/10.1016/j.chom.2021.03.005.

Chi, X., Yan, R., Zhang, J., Zhang, G., Zhang, Y., Hao, M., et al. (2020). A neutralizing human antibody binds to the N-terminal domain of the spike protein of SARS-CoV-2. *Science*, *369*, 650–655. https://doi.org/10.1126/science.abc6952.

Corti, D., Purcell, L. A., Snell, G., & Veesler, D. (2021). Tackling COVID-19 with neutralizing monoclonal antibodies. *Cell*, *184*, 4593–4595. https://doi.org/10.1016/j.cell.2021.07.027.

Emsley, P., Lohkamp, B., Scott, W. G., & Cowtan, K. (2010). Features and development of coot. *Acta Crystallographica. Section D, Biological Crystallography*, *66*, 486–501. https://doi.org/10.1107/S0907444910007493.

Fan, X., Cao, D., Kong, L., & Zhang, X. (2020). Cryo-EM analysis of the post-fusion structure of the SARS-CoV spike glycoprotein. *Nature Communications*, *11*, 3618. https://doi.org/10.1038/s41467-020-17371-6.

Ke, Z., Oton, J., Qu, K., Cortese, M., Zila, V., Mckeane, L., et al. (2020). Structures and distributions of SARS-CoV-2 spike proteins on intact virions. *Nature*, *588*, 498–502. https://doi.org/10.1038/s41586-020-2665-2.

Liu, L., Iketani, S., Guo, Y., Chan, J. F., Wang, M., Liu, L., et al. (2022). Striking antibody evasion manifested by the omicron variant of SARS-CoV-2. *Nature*, *602*, 676–681. https://doi.org/10.1038/s41586-021-04388-0.

Liu, L., Wang, P., Nair, M. S., Yu, J., Rapp, M., Wang, Q., et al. (2020). Potent neutralizing antibodies against multiple epitopes on SARS-CoV-2 spike. *Nature*, *584*, 450–456. https://doi.org/10.1038/s41586-020-2571-7.

Lyngse, F. P., Molbak, K., Skov, R. L., Christiansen, L. E., Mortensen, L. H., Albertsen, M., et al. (2021). Increased transmissibility of SARS-CoV-2 lineage B.1.1.7 by age and viral load. *Nature Communications*, *12*, 7251. https://doi.org/10.1038/s41467-021-27202-x.

Mannar, D., Saville, J. W., Zhu, X., Srivastava, S. S., Berezuk, A. M., Tuttle, K. S., et al. (2022). SARS-CoV-2 omicron variant: Antibody evasion and cryo-EM structure of spike protein-ACE2 complex. *Science*, *375*, 760–764. https://doi.org/10.1126/science.abn7760.

Mlcochova, P., Kemp, S. A., Dhar, M. S., Papa, G., Meng, B., Ferreira, I., et al. (2021). SARS-CoV-2 B.1.617.2 Delta variant replication and immune evasion. *Nature*, *599*, 114–119. https://doi.org/10.1038/s41586-021-03944-y.

Ozono, S., Zhang, Y., Ode, H., Sano, K., Tan, T. S., Imai, K., et al. (2021). SARS-CoV-2 D614G spike mutation increases entry efficiency with enhanced ACE2-binding affinity. *Nature Communications*, *12*, 848. https://doi.org/10.1038/s41467-021-21118-2.

Pallesen, J., Wang, N., Corbett, K. S., Wrapp, D., Kirchdoerfer, R. N., Turner, H. L., et al. (2017). Immunogenicity and structures of a rationally designed prefusion MERS-CoV spike antigen. *Proceedings of the National Academy of Sciences of the United States of America*, *114*, E7348–E7357. https://doi.org/10.1073/pnas.1707304114.

Pettersen, E. F., Goddard, T. D., Huang, C. C., Couch, G. S., Greenblatt, D. M., Meng, E. C., et al. (2004). UCSF Chimera—A visualization system for exploratory research and analysis. *Journal of Computational Chemistry*, *2004*(5), 1605–1612. https://doi.org/10.1002/jcc.20084.

Pettersen, E. F., Goddard, T. D., Huang, C. C., Meng, E. C., Couch, G. S., Croll, T. I., et al. (2021). UCSF ChimeraX: Structure visualization for researchers, educators, and developers. *Protein Science*, *30*, 70–82. https://doi.org/10.1002/pro.3943.

Piccoli, L., Park, Y. J., Tortorici, M. A., Czudnochowski, N., Walls, A. C., Beltramello, M., et al. (2020). Mapping neutralizing and Immunodominant sites on the SARS-CoV-2 spike receptor-binding domain by structure-guided high-resolution serology. *Cell*, *183*, 1024–1042. https://doi.org/10.1016/j.cell.2020.09.037.

Planas, D., Veyer, D., Baidaliuk, A., Staropoli, I., Guivel-Benhassine, F., Rajah, M. M., et al. (2021). Reduced sensitivity of SARS-CoV-2 variant Delta to antibody neutralization. *Nature*, *596*, 276–280. https://doi.org/10.1038/s41586-021-03777-9.

Plante, J. A., Liu, Y., Liu, J., Xia, H., Johnson, B. A., Lokugamage, K. G., et al. (2021). Spike mutation D614G alters SARS-CoV-2 fitness. *Nature*, *592*, 116–121. https://doi.org/10.1038/s41586-020-2895-3.

Punjani, A., & Fleet, D. J. (2021). 3D variability analysis: Resolving continuous flexibility and discrete heterogeneity from single particle cryo-EM. *Journal of Structural Biology*, *213*, 107702. https://doi.org/10.1016/j.jsb.2021.107702.

Punjani, A., Rubinstein, J. L., Fleet, D. J., & Brubaker, M. A. (2017). cryoSPARC: algorithms for rapid unsupervised cryo-EM structure determination. *Nature Methods*, *14*, 290–296. https://doi.org/10.1038/nmeth.4169.

Scheres, S. H. W. (2012). RELION: Implementation of a Bayesian approach to cryo-EM structure determination. *Journal of Structural Biology*, *180*, 519–530. https://doi.org/10.1016/j.jsb.2012.09.006.

Scheres, S. H. W. (2016). Chapter Six—Processing of structurally heterogeneous cryo-EM data in RELION. *Methods in Enzymology*, *579*, 125–157. https://doi.org/10.1016/bs.mie.2016.04.012.

Shang, J., Wan, Y., Luo, C., Ye, G., Geng, Q., Auerbach, A., et al. (2020). Cell entry mechanisms of SARS-CoV-2. *Proceedings of the National Academy of Sciences of the United States of America*, *117*, 11727–11734. https://doi.org/10.1073/pnas.2003138117.

Su, S. C., Yang, T. J., Yu, P. Y., Liang, K. H., Chen, W. Y., Yang, C. W., et al. (2021). Structure-guided antibody cocktail for prevention and treatment of COVID-19. *PLoS Pathogens*, *17*, e1009704. https://doi.org/10.1371/journal.ppat.1009704.

Walls, A. C., Park, Y. J., Tortorici, M. A., Wall, A., Mcguire, A. T., & Veesler, D. (2020). Structure, function, and antigenicity of the SARS-CoV-2 spike glycoprotein. *Cell*, *181*, 281–292. https://doi.org/10.1016/j.cell.2020.02.058.

Wang, P., Casner, R. G., Nair, M. S., Wang, M., Yu, J., Cerutti, G., et al. (2021). Increased resistance of SARS-CoV-2 variant P.1 to antibody neutralization. *Cell Host & Microbe*, *29*, 747–751. https://doi.org/10.1016/j.chom.2021.04.007.

Wang, P., Nair, M. S., Liu, L., Iketani, S., Luo, Y., Guo, Y., et al. (2021). Antibody resistance of SARS-CoV-2 variants B.1.351 and B.1.1.7. *Nature*, *593*, 130–135. https://doi.org/10.1038/s41586-021-03398-2.

Wrapp, D., Wang, N., Corbett, K. S., Goldsmith, J. A., Hsieh, C. L., Abiona, O., et al. (2020). Cryo-EM structure of the 2019-nCoV spike in the prefusion conformation. *Science*, *367*, 1260–1263. https://doi.org/10.1126/science.abb2507.

Yang, J., Wang, W., Chen, Z., Lu, S., Yang, F., Bi, Z., et al. (2020). A vaccine targeting the RBD of the S protein of SARS-CoV-2 induces protective immunity. *Nature*, *586*, 572–577. https://doi.org/10.1038/s41586-020-2599-8.

Yang, T. J., Yu, P. Y., Chang, Y. C., & Hsu, S.-T. D. (2021). D614G mutation in the SARS-CoV-2 spike protein enhances viral fitness by desensitizing it to temperature-dependent denaturation. *The Journal of Biological Chemistry*, *297*, 101238. https://doi.org/10.1016/j.jbc.2021.101238.

Yang, T. J., Yu, P. Y., Chang, Y. C., Liang, K. H., Tso, H. C., Ho, M. R., et al. (2021). Effect of SARS-CoV-2 B.1.1.7 mutations on spike protein structure and function. *Nature Structural & Molecular Biology*. https://doi.org/10.1038/s41594-021-00652-z.